JOURNAL OF MATERIALS SCIENCE 21 (1986) 1417–1422

Characterization of creep cavity shape in hot-pressed silicon carbide using small-angle neutron scattering

R. A. PAGE
Southwest Research Institute, San Antonio, Texas 78284, USA
S. SPOONER
Oak Ridge National Laboratory, Oak Ridge, Tennessee 37830, USA

Fine-grained silicon carbide with a continuous second-phase grain-boundary film was crept under compressive loading at 1600° C. The shape of the resultant grain-boundary cavities was characterized using small-angle neutron scattering. During the early stages of creep the cavities grew more rapidly in the plane of the grain boundary, as evidenced by an elongation of the isointensity contours and an increase in the radius of gyration, R_D, along the direction of the applied compressive stress. During the latter stages of creep the cavities grew more rapidly perpendicular to the grain-boundary plane, as evidenced by a gradual reduction in the scattering anisotropy and by an increase in R_D perpendicular to the compressive stress axis relative to R_D parallel to the compressive stress axis. Cavity aspect ratios calculated from the ratios of the R_D values parallel to and perpendicular to the compressive stress axis are shown to support a recent model of cavity growth in a viscous grain-boundary film.

1. Introduction

The high relative strength and toughness of liquid-phase sintered ceramics make these materials primary candidates for high-temperature application. However, a major concern in their use is premature creep failure resulting from grain-boundary cavitation, which, in liquid-phase sintered ceramics, is thought to occur by a viscous growth process [1] taking place entirely within the grain-boundary glassy phase [2].

A recent model of viscous creep cavity growth [3] indicates that the morphology of evolving cavities will depend on the ratios R/l and R_0/l, where R is the instantaneous cavity radius, R_0 is the initial cavity radius and $2l$ is the cavity spacing. For small R_0/l, i.e. widely spaced cavities, growth in the plane of the boundary occurs much more rapidly than growth perpendicular to the boundary. Thus, the cavities quickly assume a crack-like morphology and maintain this morphology until coalescence occurs. For larger R_0/l, i.e. more closely spaced cavities, growth in the plane of the boundary is initially more rapid than growth perpendicular to the plane; this ranking is eventually reversed as growth progresses. Hence the cavities initially develop as oblate spheroids with aspect ratios increasing with growth, and then cavities return to a spherical shape as growth progresses.

Qualitative support for the behaviour outlined above has been obtained from small-angle neutron scattering (SANS) measurements of a crept hot-pressed silicon carbide [4]. Scattering anisotropy in these SANS data [4] has been analysed to obtained a quantitative measure of cavity aspect ratio as a function of creep strain. The results of this analysis are compared with theoretical predictions.

2. Experimental details

2.1. Material

A hot-pressed silicon carbide (NC 203 from Norton Co., Worcester, Massachusetts) was used in this investigation. Metallography showed that the grains were equiaxed, the grain size ranged from 3 to 5 μm, and the microstructure was basically pore-free. Previous X-ray characterization by McHenry and Tressler [5] showed that the ceramic consisted of $< 5\%$ β-SiC, $\approx 5\%$ WC (from the cobalt-bonded tungsten carbide ball milling debris), and 90% hexagonal α-SiC polytypes 2H, 4H and 6H. It has been suggested [5–7] that most of the chemical impurities in the material (aluminium, oxygen, calcium, zirconium and titanium) are present as an amorphous, continuous grain-boundary film. This has been confirmed by Auger [4] and TEM and microprobe [8] work, which show that the grain-boundary second phase was glassy material enriched in the above-mentioned impurity elements.

2.2. Creep tests

Compression creep tests were performed on right circular cylinders, 6.4 mm in diameter and 12.7 mm long, at 1600° C in a titanium gettered argon environment. Two stress levels, 570 and 605 MPa, and test durations ranging from 6×10^2 to 1.33×10^5 sec were employed in the cavitation study. Upon completion of the creep tests the specimens were rapidly

0022–2461/86 $03.00 + .12

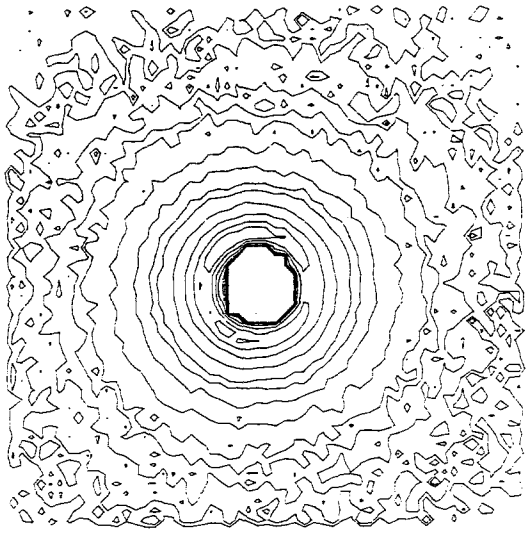

Figure 1 Isointensity contour plot of SANS data from an as-received sample of hot-pressed silicon carbide.

cooled to room temperature before being unloaded, thus freezing-in the cavity size and shape present at the end of the creep test.

2.3. SANS measurements

Rectangular flats, 5 mm × 12.7 mm, were ground and polished on opposite sides of the specimens following creep. This procedure yielded specimens approximately 3.7 mm thick, as measured between the parallel flats. Final polishing was performed so that grain pullout was minimized. An as-received control sample and a sample held at 1600° C for 3.6×10^4 sec under zero load were prepared in a similar fashion.

The small-angle scattering measurements, which were performed on the 30 m instrument at the National Center for Small-Angle Scattering Research at Oak Ridge National Laboratory [9], utilized an incident neutron wavelength, λ, of 0.475 nm and sample-to-detector distances of 9 and 16.5 m. This yielded intensity data at scattering vectors, q, from 0.036 to 0.2 nm^{-1}, where $q = 4\pi \sin\theta/\lambda$ and θ is the Bragg angle. Background scattering arising from electronic background, scattering from the empty specimen holder and non-uniform detector sensitivity was removed as described earlier [10]. Corrected scattering was calibrated with the scattering from a well-characterized irradiated aluminium sample [11] containing voids.

3. Results and discussion

Experimental evidence [4] suggests that the scattering intensity increase observed during creep of the SiC was due to the nucleation and growth of grain-boundary cavities. Determination of the cavity sizes and numbers has been presented [4]. In this paper the SANS measurements are used to examine the shapes of the evolving cavities. This is possible because the two-dimensional scattering pattern depends on the size, shape and orientation of the scattering centres, which in our case are considered to be grain-boundary cavities. Anisotropy in the two-dimensional scattering pattern specifically indicates the presence of non-spherical scatterers possessing a degree of preferred orientation.

Scattering from an uncrept specimen, from here on referred to as the blank, was isotropic over the entire angular range investigated (Fig. 1) as is expected from a random polycrystalline material. To identify any scattering anisotropy developed during creep the scattering from the blank was subtracted from each of the crept specimens. The remaining scattering intensity arises primarily from the presence of creep cavities [4]. The dramatic effect that blank subtraction may have on the scattering pattern is illustrated in Fig. 2. Prior to subtraction, the scattering from a sample crept at 605 MPa for 0.75 h (Fig. 2a) shows only a slight anisotropy. After subtraction, however, a strong anisotropy is evident (Fig. 2b). All scattering discussed from this point on has undergone subtraction of the scattering from the blank specimen.

Qualitative information about cavity shape can be obtained from isointensity contours of the crept specimens (Fig. 3). It is evident from these figures that anisotropic scattering developed during the early stages of creep (Fig. 3a). The degree of anisotropy increased up to a strain of approximately 0.5%

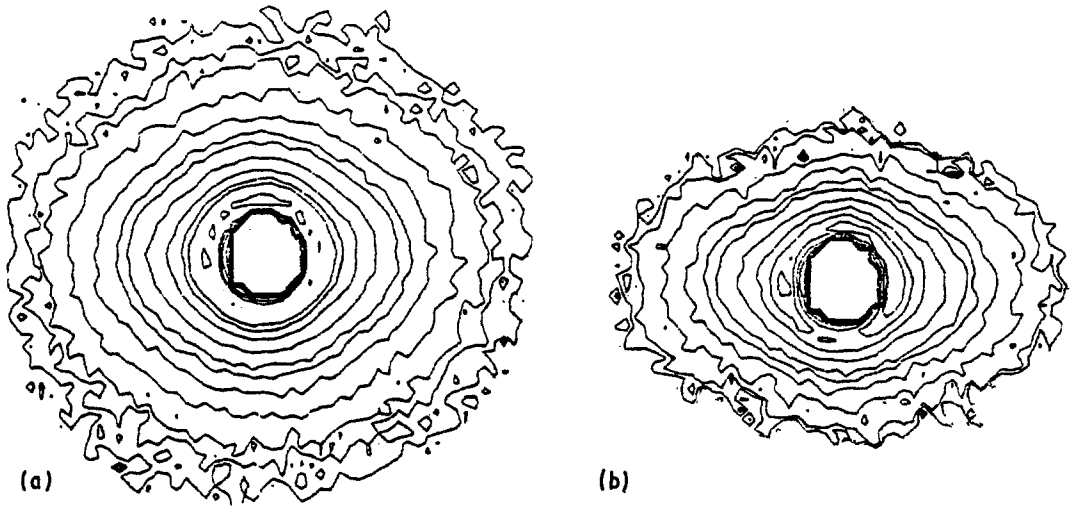

Figure 2 Isointensity contour plots of SANS data from a silicon carbide sample crept to a strain of 0.523% (a) before and (b) after subtraction of the scattering from the as-received sample.

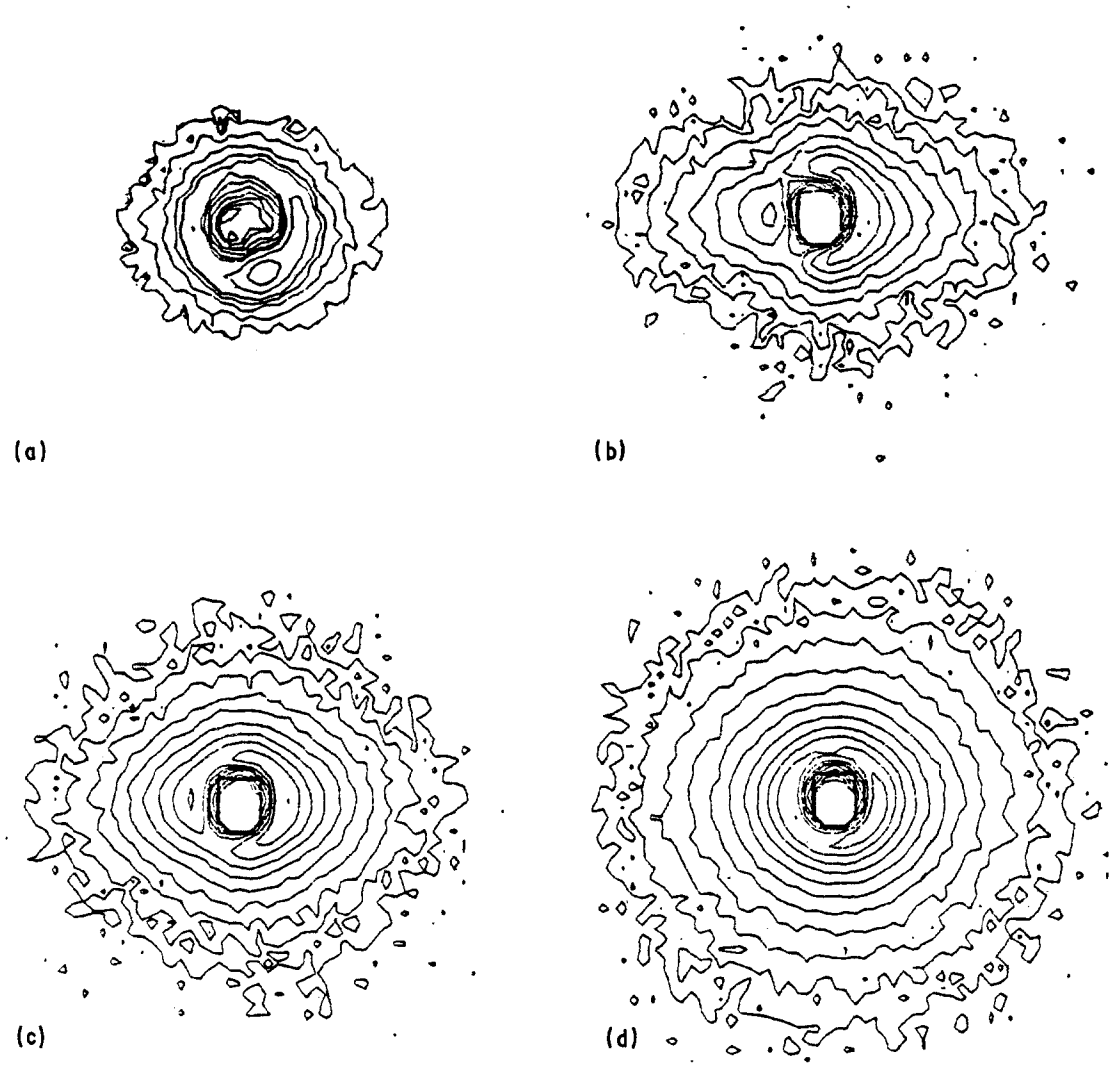

Figure 3 Isointensity contour plots (blank subtracted) illustrating progression in scattering anisotropy during compressive creep. Strains (a) 0.188%, (b) 0.408%, (c) 0.865%, (d) 1.87%.

(Fig. 3b). Scattering patterns from samples crept to progressively higher strains showed a gradual reduction in the degree of anisotropy. This continued throughout creep, so that by the final stages of creep the two-dimensional scattering patterns were practically isotropic (Fig. 3d).

Graphs of intensity against azimuthal angle within a ring of constant q (Fig. 4) show that the scattering patterns were elongated perpendicular to the loading axis throughout the entire q range investigated. The enhancement of intensity in the direction perpendicular to the compressive stress axis indicates an elongation of the cavities in the direction parallel to the compressive stress axis. Since cavitation is assumed to occur on boundaries which are subject to a net tensile stress, i.e. boundaries which are parallel to the compressive stress axis, the observed anisotropy corresponds to cavity elongation in the plane of the grain boundary.

An estimate of the degree of cavity elongation can be obtained by constructing intensity against q slices both parallel and perpendicular to the applied stress direction. A series of intensity profiles developed in such a manner are presented in Fig. 5. From these data it is possible to calculate the radius of gyration*, R_D, both perpendicular and parallel to the direction of the applied stress (Table I). Assuming ellipsoidal cavities, the ratios of these R_D values would then provide an estimate† of the aspect ratio of the cavities. Such aspect ratios are presented in Fig. 6. These data show that the cavities start as spheres but quickly develop into ellipsoids, reaching a minimum aspect ratio of approximately 0.75 at a creep strain of approximately 0.5%. The aspect ratio increases gradually beyond this point, approaching a value of 1.0 (spherical cavities) at a strain of approximately 3%.

The evolution of cavities from spheres to ellipsoids and then back to spheres has been predicted by theory [3]. Although the theory and experiments qualitatively agree, significant quantitative differences are evident from Fig. 6. The experimental data indicate that the development of ellipsoidal cavities occurs much more rapidly than predicted. This discrepancy could be due to the use of R_D values in calculating the aspect ratio.

*The definition of R_D and the method used for its determination are presented in the Appendix.

†Due to the distribution of cavity orientations present in a polycrystalline material, the aspect ratios calculated in this manner overestimate the actual ratios, with the degree of overestimation increasing as the deviation from a ratio of unity increases.

TABLE I Cavity shape parameters calculated from the SANS data

Stress (MPa)	Strain (%)	t (h)	$R_{d\perp}$* (nm)	$R_{d\parallel}$† (nm)	Aspect ratio‡
570	0.188	0.17	41.9	44.0	0.953
570	0.408	3.0	36.8	49.5	0.743
570	0.704	6.0	41.8	50.1	0.834
570	0.865	12.0	43.0	50.3	0.855
570	1.87	25.0	49.0	51.9	0.944
570	1.89	37.0	49.7	52.3	0.950
605	0.181	0.17	40.0	42.5	0.941
605	0.523	0.75	43.6	56.4	0.773
605	0.644	3.0	38.7	49.1	0.788
605	1.15	6.0	47.1	51.8	0.909
605	1.69	12.0	48.9	51.6	0.948
605	3.10	25.0	51.0	51.1	0.998

*Radius of gyration perpendicular to the compressive stress axis.
†Radius of gyration parallel to the compessive stress axis.
‡Aspect ratio is defined as $R_{D\perp}/R_{D\parallel}$.

As indicated in the Appendix, R_D represents a moment of the cavity-size distribution that is heavily weighted towards the high end of the distribution. The experimental aspect ratios are thus representative of the larger and more mature cavities in the population. One would expect that shape changes in these cavities would occur at earlier times than in cavities that either nucleated at a later time or grew at a slower rate.

A difference in the manner in which the two curves return to an aspect ratio of unity is also apparent from Fig. 6. The experimental data appear to asymptotically approach an aspect ratio of unity, while the theoretical curve displays a nearly vertical slope and predicts the development of aspect ratios much greater than unity, i.e. cavities elongated perpendicular to the grain boundary plane. The theoretical model does not permit cavity coalescence, however. Therefore, as the ligament between adjacent cavities becomes quite small, cavities with large aspect ratios are produced. If a statistical treatment of cavity coalescence were included in the model, an aspect ratio limit near unity should occur with the limit being approached asymptotically, as observed in the experimental data.

A critical test of the model could be performed if the aspect ratios of the smaller cavities were also available. Although the two-dimensional scattering patterns contain this information in principle, there is difficulty in extracting this information unambiguously. In a cavitating polycrystalline ceramic the cavities are expected to have a distribution of sizes due to continuous nucleation (4, 12, 13) and non-uniform grain-boundary normal stresses. There will also be a distribution of shapes due to variations in cavity spacing combined with variations in the time of nucleation. And finally, there will be a distribution in orientation due to the orientation distribution of the cavitating grain boundaries. For the case of single scattering from independent cavities the scattered intensity, $i(\boldsymbol{q})$, is given by

$$i(\boldsymbol{q}) = \int_1^\infty \int_0^\infty \int_0^{\pi/2} N(w)\,N(R)\,N(\theta)\,\Phi(w, R, \theta, q)\,\mathrm{d}\theta\,\mathrm{d}R\,\mathrm{d}w \quad (1)$$

where $\boldsymbol{q}$ is the scattering vector, $\Phi(w, R, \theta, q)$ is the scattered intensity from a cavity of shape w, size R, and orientation θ, and $N(w)$, $N(R)$ and $N(\theta)$ are the shape, size, and orientation distributions, respectively. The above formulation represents the simplest case where the distribution functions are independent of each other. It is more realistic to assume that each of the distribution functions would be correlated.

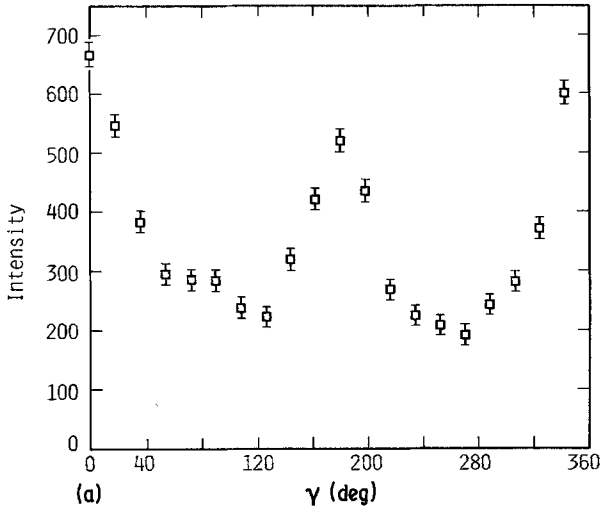

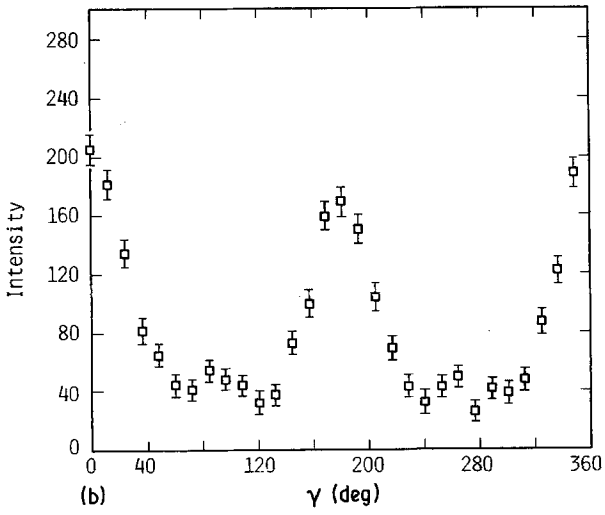

Figure 4 Intensity against angle for rings of constant q of (a) $q = 0.05\,\mathrm{nm}^{-1}$, (b) $q = 0.07\,\mathrm{nm}^{-1}$ and (c) $q = 0.10\,\mathrm{nm}^{-1}$. Inset in (c) illustrates relationship between the angle γ and the compressive stress axis.

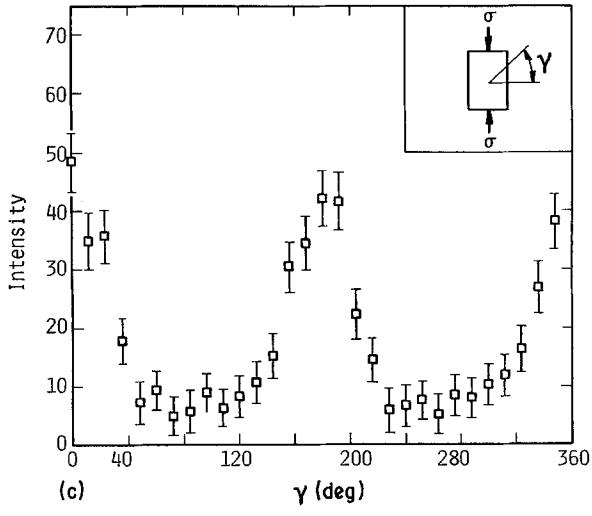

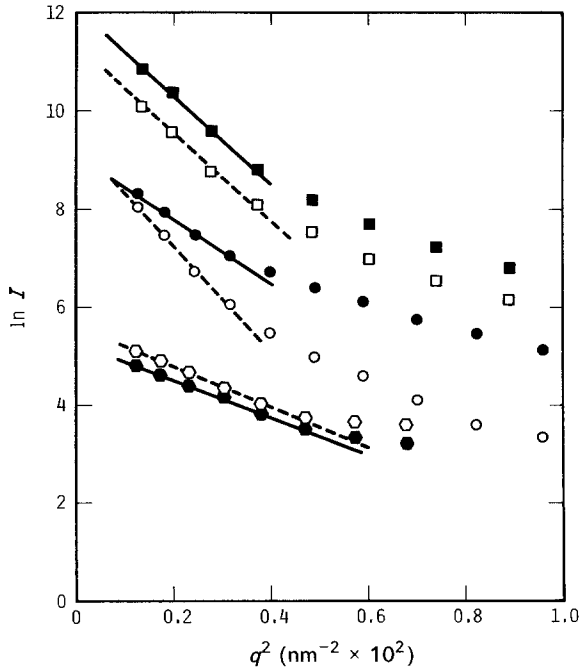

Figure 5 Plot of ln I against q^2 for slices taken parallel (open points) and perpendicular (closed points) to the compressive stress axis. Strains (○, ●) 0.18%; (○, ●) 0.52%; (□, ■) 3.1%.

Although numerous solutions for the three distribution functions can be obtained by fitting experimental two dimensional data to Equation 1, no unique set of structural parameters can be expected. This is the same problem as that encountered in trying to determine both the shape and the size distribution from one-dimensional data [14]. It would be necessary to assume a particular shape in order to calculate the size distribution. In the same manner, it would be necessary to know two of the distribution functions in Equation 1 in order to uniquely determine the third. Unfortunately, our present understanding of the cavitation process precludes this possibility.

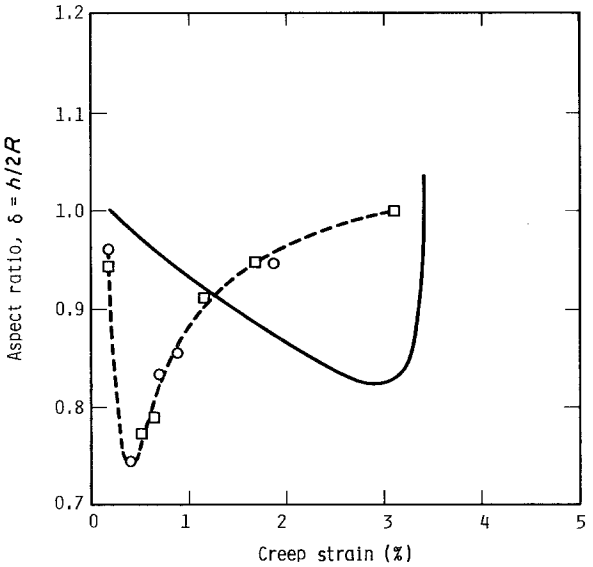

Figure 6 Cavity aspect ratio against creep strain for hot-pressed silicon carbide. Open data points are from SANS measurements. Solid curve is a theoretical prediction from Chan *et al.* [3]. Stresses (○) 570 MPa, (□) 605 MPa.

4. Conclusions

The following conclusions concerning creep cavitation in silicon carbide containing a continuous grain-boundary film can be drawn from the results of the present investigation.

1. During the initial stages of creep, cavity growth in the plane of the grain boundary is more rapid than growth perpendicular to the boundary. At some intermediate stage, the cavity growth rate perpendicular to the boundary exceeds that parallel to the boundary, resulting in a reduction in the aspect ratio of the cavities during the latter stages of creep.

2. The evolution in cavity morphology identified by the SANS results agrees with the predictions of the viscous cavity growth model of Chan *et al.* [3]. It should be noted that the cavity morphology is predicted to be sensitive to the cavity spacing. Hence, the results observed in this study should be considered as representative of cavity growth under conditions which have produced closely spaced cavities. An alteration of the creep conditions, so that cavities nucleate with a large separation, would be expected to change the growth morphology as well.

3. The inhomogenous nature of the creep cavitation process in a random polycrystalline material produces cavities with a distribution of sizes, shapes, and orientations. It is not possible to obtain unique solutions for each of these distribution functions from analysis of the two-dimensional SANS scattering alone.

Acknowledgements

The authors are grateful for the support of this work by the Department of Energy, Office of Basic Energy Sciences under Grant. No. DE–FGO5–84ER45063. We also thank the staff of the National Center for Small-Angle Scattering Research for their individual assistance in this project.

Appendix

For a homogeneous particle, the radius of gyration is defined as

$$R_D^2 = \frac{1}{V_p}\int_{V_p} r_D^2 S(r_D)\mathrm{d}r_D \qquad \text{(A1)}$$

where $S(r_D)$ is the cross-sectional area of the particle along a plane normal to the direction D at a distance r_D from the centre of gravity of the particle, V_p is the volume of the particle and D is in the plane perpendicular to the incident neutron wave vector. For an ensemble of scattering centres of various sizes, such as expected in these experiments, R_D represents a moment of the size distribution weighted heavily toward the largest scatterers.

For small values of q ($qa \leqslant 1.2$, where a is the cavity radius) Guinier [15] has shown that

$$\sum(q) = e^{-q^2 R_D^2} \qquad \text{(A2)}$$

where $\sum(q)$ is the scattering function in the plane defined by the incident neutron wave vector and D. Thus, the scattered intensity, I, in the Guinier region

can be written as

$$\ln(I) = A - q^2 R_D^2/3 \qquad \text{(A3)}$$

where A is a constant. Hence, a plot of $\ln(I)$ against q^2 should fit a straight line of slope $-R_D^2/3$. Experimental values of R_D (presented in Table I) were determined by fitting the scattering data for $0.036\,\text{nm}^{-1} \leqslant q \leqslant 0.057\,\text{nm}^{-1}$ to Equation A3.

References

1. A. G. EVANS and A. RANA, *Acta Metall.* **28** (1980) 129.
2. J. E. MARION, A. G. EVANS, M. D. DRORY and D. R. CLARKE, *ibid.* **31** (1983) 1445.
3. K. S. CHAN, J. LANKFORD and R. A. PAGE, *ibid.* **32** (1984) 1907.
4. R. A. PAGE, J. LANKFORD and S. SPOONER, *ibid.* **32** (1984) 1275.
5. K. D. MCHENRY and R. E. TRESSLER, *J. Amer. Ceram. Soc.* **63** (1980) 152.
6. A. G. EVANS and F. F. LANGE, *J. Mater. Sci.* **10** (1975) 1659.
7. F. F. LANGE, *ibid.* **10** (1975) 314.
8. G. Q. WEAVER and B. A. OLSON, in "High Strength Silicon Carbide for Use in Severe Environments," (Norton Company, Worcester, Massachusetts, 1973).
9. W. C. KOEHLER and R. W. HENDRICKS, *J. Appl. Phys.* **50** (1979) 1951.
10. R. A. PAGE, J. R. WEERTMAN and M. ROTH, *Acta Metall.* **30** (1982) 1357.
11. R. W. HENDRICKS, J. SCHELTEN and W. SCHMATZ, *Phil. Mag.* **30** (1974) 819.
12. R. A. PAGE and J. LANKFORD, *J. Amer. Ceram. Soc.* **66** (1983) C146.
13. R. A. PAGE, J. LANKFORD and S. SPOONER, *J. Mater. Sci.* **19** (1984) 3360.
14. G. KOSTORZ, in "Treatise on Materials Science and Technology", edited by H. Herman, Vol. 15 (1979) p. 227.
15. A. GUINIER, *Ann. Phys. Paris* **12** (1939) 161.

Received 16 May
and accepted 12 June 1985